Draft version May 19, 2016
Preprint typeset using LaTeX style AASTeX6 v. 1.0

OBSERVATIONS OF MOLECULAR OUTFLOW FROM POLAR JETS IN THE LKHα 225S PROTOPLANETARY DISK

Sean Sellers
Vassar College
124 Raymond Avenue
Poughkeepsie, NY 12604, USA

ABSTRACT

Observations of molecular outflow associated with protoplanetary disks reveal details about the composition, history, and dynamics of pre-main sequence stellar objects. We present molecular absorption line data for several regions of the Herbig Ae/Be protostellar source LkHα 225S. Spectra for ^{12}CO, ^{13}CO and H_2O were taken using the NIRSPEC infrared spectrograph on the Keck II telescope in the M band and the L band. We detect absorption from ^{12}CO, ^{13}CO, and H_2O. The ^{12}CO lines have a blueshift of 83.36 km/s, while the ^{13}CO lines have a blueshift of 39.87 km/s. Absorption lines in H_2O show a blueshift of approximately 31 km/s, implying that the three molecules are found in different regions of the LkHα 225S system. Identification of specific properties of the protostellar object is significantly complicated by the large distance to the regions, as well as several clouds along the line of sight to the region, making the molecular-derived properties of the outflow that much more significant.

1. INTRODUCTION

Bipolar outflow is an integral part of star formation, allowing the protostellar accretion disk to shed angular momentum and finish its collapse (Bally et al. 1996). The consequences of these outflows have been observable for more than half a century as Herbig-Haro objects: bow shocks with characteristic emission spectra. As outflows appear to be present in all types of protostars, from brown dwarfs to O-type stars, emission and absorption from these regions are important in detecting embedded star-forming regions, as well as understanding the evolution of the protoplanetary disk.

In the current favored model, the inner regions of these outflows experience a significant radiative acceleration along the column of the outflow region (Kurosawa et al. 2005). In addition to the linear accelaration along the outflow, these regions also exhibit a spiraling motion, from the conservation of angular momentum originating in the rotation of the disk. The underlying physics of these regions, however, are not well understood. While there are several models for bipolar outflow from a protoplanetary disk, the physical process driving these outflows is not known, and the precise physical processes occuring in these regions is often obscure.

In this paper, we consider the molecular outflow from the Herbig Ae/Be (HAeBe) source, LkHα 225S (also known as V1318 Cyg). Herbig Ae/Be stars are intermediate-mass pre-main sequence stars with $1.5 \leq M/M_\odot \leq 10$ (Herbig 1960; Herbst & Shevchenko 1999), and signs of infrared excess indicating the presence of dust in a protoplanetary disk. We present observations of ^{12}CO and ^{13}CO in the 4.94 to 5.1 μm range, as well as H_2O observations in the 2.85 to 3.65 μm range. Our observations reveal several regions, and interesting properties of the bipolar outflow assiciated with LkHα 225S. Our observations and data reduction techniques are described in Section 2. Analysis of our data and procedures are found in Section 3. Discussion about this region, and recommended future work can be found in Section 4. Further discussion and conclusions are found in Section 5.

2. OBSERVATIONS AND DATA REDUCTION

Our data were obtained using the NIRSPEC infrared echelle spectrograph on the Keck II telescope. Data were taken for CO in December of 2006 and July of 2009. The December observations had a total integration time of 30 seconds in 1 setting, while the July observations had a total of 4 minutes of integration time in each of 2 settings. Observations of H_2O were taken in July 2009. These observations had a total exposure time of 12 minutes in each of two settings (Salyk et al. 2008).

The telescope was directed toward LkHα 225S at $\alpha_{J2000} = 20^h20^m30.46^s$, $\delta_{J2000} = +41°21'26.8°$. Data were obtained for the wavelength range of 2.85 to 3.65

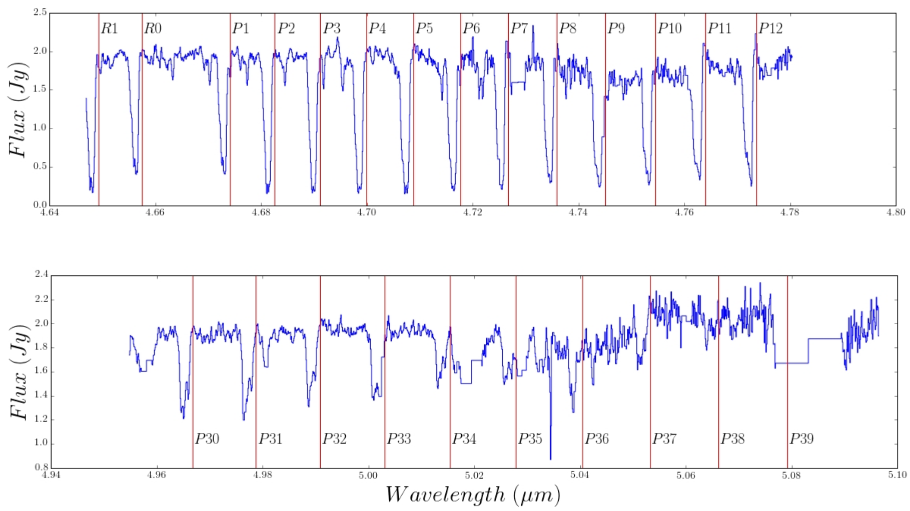

Figure 1. The obtained ^{12}CO spectrum for LkHα 225S, with the theoretical absorption locations overlaid. The portion of the spectrum between 4.78 and 4.95 μm was rejected as having poor atmospheric transparency. Despite significant noise in the spectrum, absorption lines up until the relatively high-energy P38 transition are clearly visible, as well as clearly significantly blue-shifted.

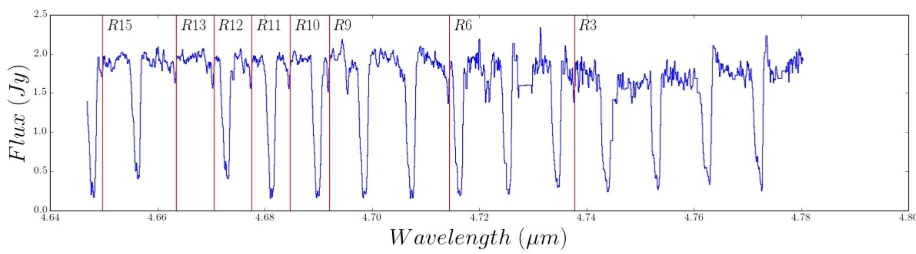

Figure 2. The same obtained spectrum for LkHα 225S, overlaid with ^{13}CO line positions in red. To prevent ambiguity as to which features are referenced, this spectrum has been slightly shifted to correct for an outflow speed of ≈ -40 km/s. The uncorrected overlay can be found as Figure 12.

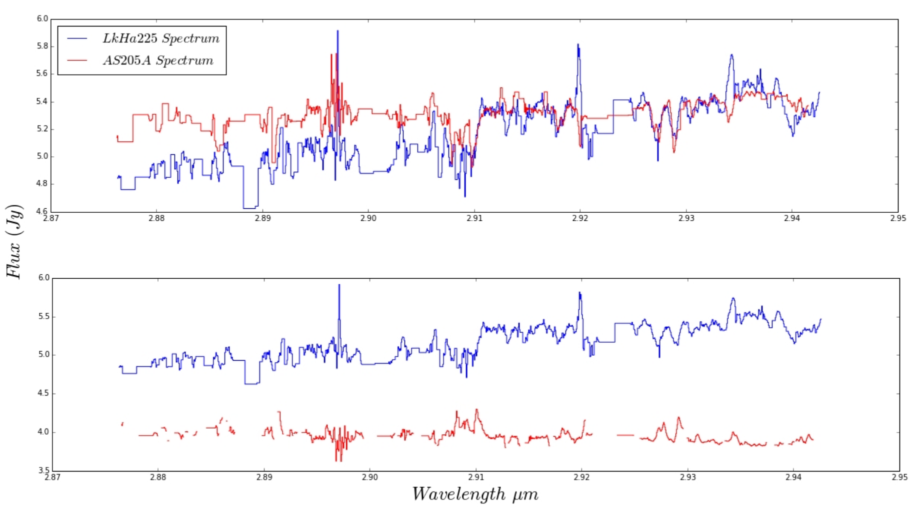

Figure 3. TOP: Overlaid 2.9 μm spectra showing H_2O features for AS 205A and LkHα 225S. In this image, the AS 205A spectrum has been inverted and shifted to align with the LkHα 225S spectrum. The necessary shift was $\approx -3 \times 10^{-4}$ μm.
BOTTOM: The same overlay, before applying the inversion and shift to the AS 205A spectrum in order to provide direct comparison with LkHα 225S.
These plots have been corrected for the source velocities of both LkHα 225S and AS 205A.

μm, and at the wavelength range of 4.64 to 5.1 μm, both with a resolution $R = 25000$ (12.5 km/s). Portions of the spectrum affected by poor atmospheric transmission were removed from the reduced data. Data were given in terms of flux density, in units of Janskys (Jy) at each wavelength bin, resulting in a high resolution spectrum for a wide wavelength range.

^{12}CO transitions were observed in the 4.64 to 5.1 μm wavelength range for several P-branch ($\Delta J = -1$) rovibrational transitions, and one R-branch ($\Delta J = +1$) transition. A second R-branch transition is visible in the spectrum, as seen in Figure 1, but is incomplete. In order to provided detailed analysis of the region, both the lower energy ($4.65 \leq \lambda \leq 4.78$) and higher energy ($4.96 \leq \lambda \lesssim 5.06$) transitions were studied.

3. ANALYSIS

Analysis of the absorption features was performed using a least-squares fitting of a Gaussian curve of the form:

$$f(x) = Ae^{-\frac{(x-b)^2}{2\sigma^2}} + C \tag{1}$$

where A is the depth (amplitude) of the well, b is the center of the well, σ is the standard deviation of the function (controlling the width), and C is the level of the continuum. This process was repeated with ^{13}CO. There were significantly fewer absorption lines available for fitting ^{13}CO due to a lower abundance, as well as interference from the more prominant ^{12}CO features. Figure 2 shows the same spectrum overlaid with the theoretical ^{13}CO feature locations.

Ultimately, we were able to successfully fit nineteen absorption lines in ^{12}CO, and eight absorption lines in ^{13}CO. A sample fit for ^{12}CO can be seen in Figure 4, and stacked interpolated absorptions features for ^{12}CO and ^{13}CO can be seen in Figures 5 and 6, respectively. All fits were performed after having corrected for a LSR source velocity of -9.465 km/s (Matthews et al. 2007)

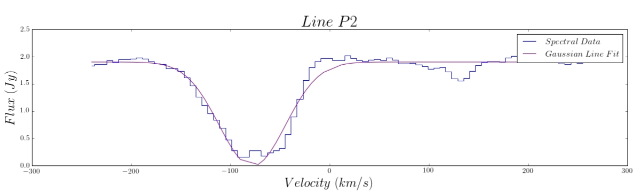

Figure 4. A sample fitting of the P(2) ^{12}CO absorption feature. Note the significant blueshifting. Visible to the right of the main feature is a small ^{13}CO absorption feature, seen here as a small dip in the continuum level. Velocities given here have been corrected for the source velocity.

Interpolation was performed in Python. The interpolated lines were then summed together to provide the lineshapes seen in Figures 5 and 6.

Having obtained a set of fit parameters for all ^{12}CO and ^{13}CO lines available to use, we first converted standard deviation to a more usable full-width at half maximum, using the formula:

$$FWHM = 2\sigma\sqrt{2\ln(2)} \tag{2}$$

From here, we can calculate the error in each FWHM using the formulae derived by Lenz and Ayres (Lenz & Ayres 1992). The formula for calculating error in a Gaussian FWHM is as follows:

$$\frac{FWHM}{\sigma_{FWHM}} = C_{FWHM}\left(\frac{FWHM}{\Delta\lambda}\right)^{1/2}\frac{f_0}{\sigma_0} \tag{3}$$

Here, the parameter C_{FWHM} is given by Lenz and Ayres as ≈ 0.70 (Lenz & Ayres 1992). The quantity f_0 is the continuum level, and σ_0 is the standard deviation of the continuum level. We calculated σ_0 for each fitted absorption feature using an ≈ 75 km/s range of the continuum unperturbed by any absorption features. The quantity $\Delta\lambda$ follows from the given resolution of the NIRSPEC spectrograph ($R = 25000 = \frac{\lambda}{\Delta\lambda}$). Having obtained these quantites, we were able to determine the error for each FWHM for both ^{12}CO and ^{13}CO.

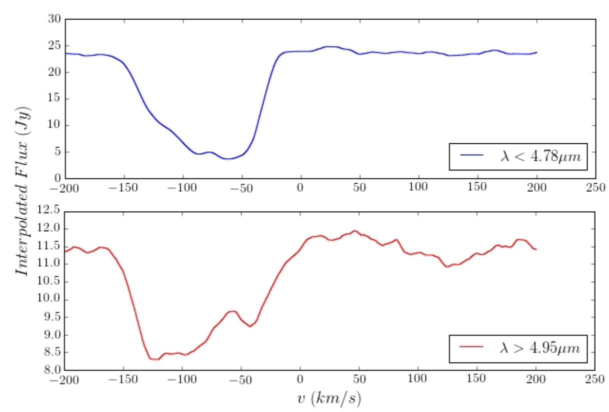

Figure 5.
TOP: Interpolated lower energy ^{12}CO lines ($\lambda < 4.78$ μm).
BOTTOM: Interpolated higher energy ^{12}CO lines ($\lambda > 4.95$ μm).
Note that both sets of stacked lines have the same double peak evident at the minima of the absorption features that persists even through interpolation.

Having determined the standard deviation of the function and the FWHM, we endeavored to also compute the equivalent width of the spectral line. For an absorption line, the width of the line is given by the rectangle with a height equal to that of the continuum level, with an area equal to the area of the Gaussian fit. Practically, the equivalent width is given by

$$W_\lambda = \int\left(1 - \frac{F_\lambda}{F_0}\right)d\lambda \tag{4}$$

$$W_\lambda = \frac{1}{F_0}\int\left(F_0 - F_\lambda\right)d\lambda \tag{5}$$

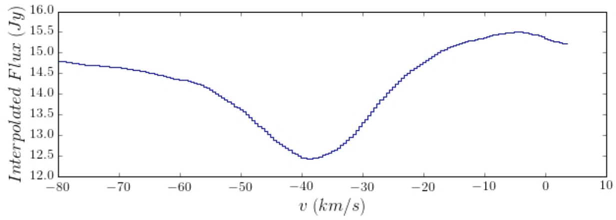

Figure 6. Interpolated ^{13}CO lines. Note that these lines do not have the double peak evident in all the observed ^{12}CO lines.

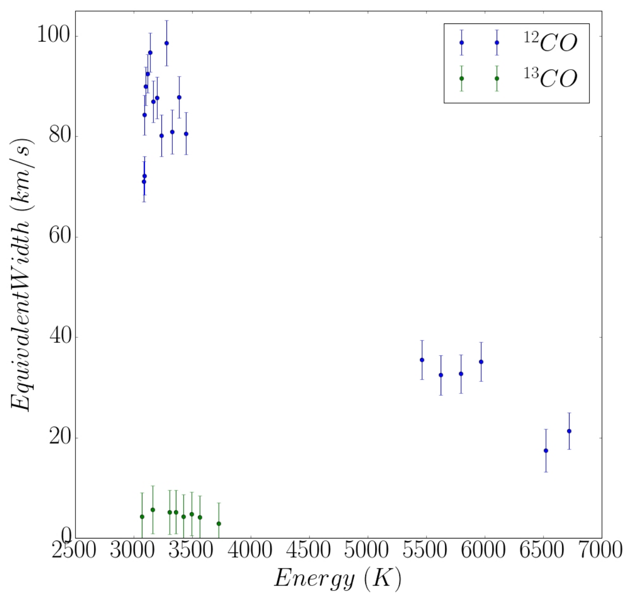

Figure 7. A plot of equivalent width against lower level energy. ^{13}CO is shown in green, while ^{12}CO is shown in blue. Note that the ^{12}CO lines are much wider than ^{13}CO at all energies.

$$W_\lambda = \frac{1}{F_0} A\sigma\sqrt{2\pi} \quad (6)$$

Here, F_0 is the continuum flux, A is the amplitude of the Gaussian, and σ is the standard deviation of the function. Error was propagated through these calculations to find the error in standard deviation, FWHM, and equivalent width. Figure 7 shows a plot of equivalent width against lower level energy in both ^{12}CO and ^{13}CO.

To determine temperature and column density of the absorbing ^{12}CO and ^{13}CO regions, we then used our data to create a rotation diagram for both isotopes of CO. Figures 8 and 9, respectively, show the rotation diagrams for ^{12} and ^{13}CO. The rotation diagrams were created using formulae found in Mundy (Mundy 1999). The rotation diagram plots $\ln(\frac{N_l}{g_l})$ against the energy of the lower level, where g_l is the lower state degeneracy, and N_l can be derived from the relationship between τ, optical depth, and the equivalent width of the well, yielding the quantity,

$$N_l = EW \frac{g_l}{g_u}\frac{8\pi\nu_o^4}{c^3}\frac{1}{A_{u\to l}} \quad (7)$$

Here, EW is the equivalent width, calculated in Eq. 6., g_u and g_l are the upper and lower state degeneracies, respectively. The frequencies (ν_0) are used here, instead of wavelength, and $A_{u\to l}$ is the Einstein-A coefficient. We can find the column density from N_l as well, using the identity,

$$N_l = N\frac{g_l}{Q(T)}e^{-\frac{E_l}{k_B T}} \quad (8)$$

Here, $Q(T)$ is the partition function. For ^{12}CO, the partition function is $Q(T)_{12} = 0.36288T\left(1 + e^{-\frac{3083.7}{T}}\right)$. For ^{13}CO, the partition function is $Q(T)_{13} = 0.6212 + 0.75758T - 5.9194\times10^{-6}T^2 + 1.5232\times10^{-8}T^3$. The degeneracy of the lower state, g_l appears in this equation again, as does the lower state energy, E_l. T is the temperature, k_B is the Boltzmann constant, and N is the column density.

Rearranging Equation 8 allows us to derive a relationship that can be plotted in terms of known quantities, which can then be used to derive further properties of the region:

$$\ln\left(\frac{N_l}{g_l}\right) = \ln\left(\frac{N}{Q(T)}\right) - \frac{E_l}{k_B T} \quad (9)$$

Which is in the form $y = B + mx$, a line, where N_l is calculated from our Gaussian fits, g_l is a known quantity for the observed transitions, as is $\frac{E_l}{k_B}$. We can plot $\ln\left(\frac{N_l}{g_l}\right)$ against $\frac{E_l}{k_B}$. The plots created for ^{12}CO can be seen in Figure 8, and ^{13}CO can be found in Figure 9. Performing a least squares fit on the linear portions of these plots allows us to calculate the rotational temperature, T_{rot} of the region from the slope of the line, and column density, N from the intercept. It is important to note that T_{rot} is not necessarily the temperature of the region, but simply the theoretical rotational temperature of the absorbing CO gas.

The final analysis performed for the CO features was an attempt to determine the source of the continuum, i.e., if the continuum was consistent with emission from the protostellar object. We used data from several sources (Hillenbrand et al. 1995; Aspin et al. 1994; Matthews et al. 2007; Palla et al. 1995) to estimate stellar parameters, in order to determine the blackbody continuum at the portion of the spectrum observed. Unfortunately, information about this object is extremely limited. Hillenbrand gives a mass of $\gtrsim 1M_\odot$, while other sources give a mass range anywhere from $\gtrsim 2M_\odot$ to

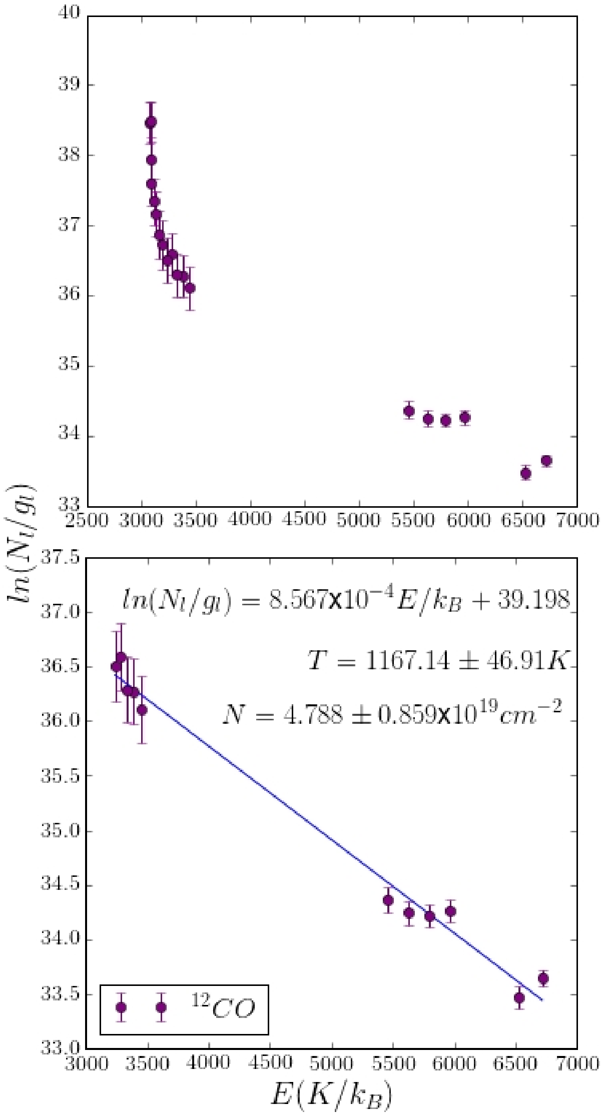

Figure 8. TOP: The full rotation diagram for ^{12}CO. BOTTOM: The apparently linear portion of the rotation diagram for ^{12}CO with linear fit and derived quantites.

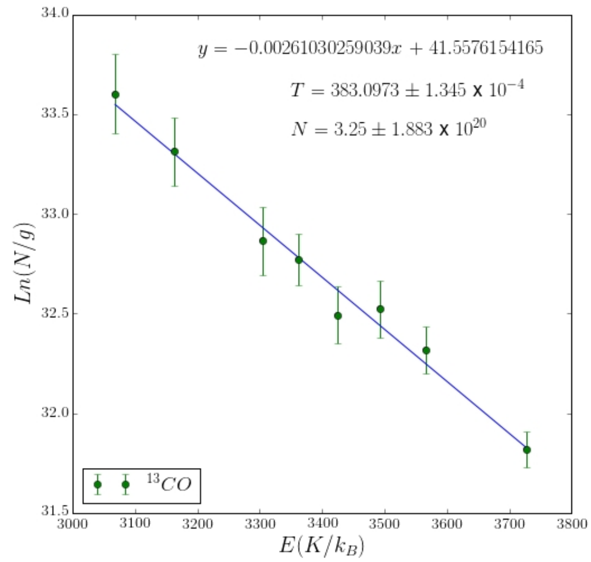

Figure 9. Rotation diagram for ^{13}CO. Note that while the rotation diagram for ^{12}CO indicates saturation, the diagram for ^{13}CO shows no saturation. Fit parameters and derived quantities are displayed on the plot.

Table 1. Theoretical Spectral Types, Temperatures, Radii

Spectral Type	Temperature (K)	Radius ($R_\odot$)
A5 V	8200	1.7
A6 V	8350	2.0
A7 V	7850	1.4
A8 V	7580	2.2
A9 V	7390	1.8
F0 V	7200	2.6
F1 V	7050	1.6
F2 V	6890	1.9
F3 V	6740	
F4 V	6590	
F5 V	6440	

$\lesssim 10 M_\odot$. No reliable information exists concerning the radius or the temperature of the protostellar object. Instead, we assumed that LkHα 225S is a pre-main sequence star of with a stellar type somewhere between $A5$ and $F5$ (Mora et al. 2001; Herbig 1960). Given this range, we were able to find temperatures corresponding to these stellar types (Kenyon & Hartmann 1995). From the temperatures, we were able to find a representative sample of radii (Fairlamb et al. 2015; Mora et al. 2001). Our representative temperatures and radii are in Table 1. Having obtained a representative sample of temperatures, we used Planck's Law to plot spectral radiance as a function of temperature:

$$B_\nu(\nu, T) = \frac{2h\nu^3}{c^2}\frac{1}{e^{\frac{h\nu}{k_B T}} - 1} \tag{10}$$

Which, given a frequency, gives us a measure of spectral radiance in W sr^{-1}m^{-2}Hz^{-1}. To convert to Jy, we applied a conversion factor to this curve of

$$\frac{1}{10^{-26}}\frac{\pi R^2}{r^2} \tag{11}$$

Where R is the radius of the object, and r is the distance to the object. This conversion factor folds in the distance scale factor and the conversion from spectral flux density in W sr^{-1} m^{-2}Hz^{-1} to Jy. We used a value of 980 pc for distance, as this is the given distance to the nearby BD +40° 4124 (Hillenbrand et al. 1995; Shevchenko et al. 1991). Extreme absorption ($A_v > 8$) along the line of sight to LkHα 225S makes direct distance measurement difficult. We applied this conversion factor to our obtained theoretical blackbody curve for the average radius, as well as the minimum and maximum radius in our spread. Ultimately, however, the given values made little difference in the final result. The distance-scaled blackbody curve for the maximum radius can be seen in Figure 10, as can the region of the curve corresponding to the measured wavelengths.

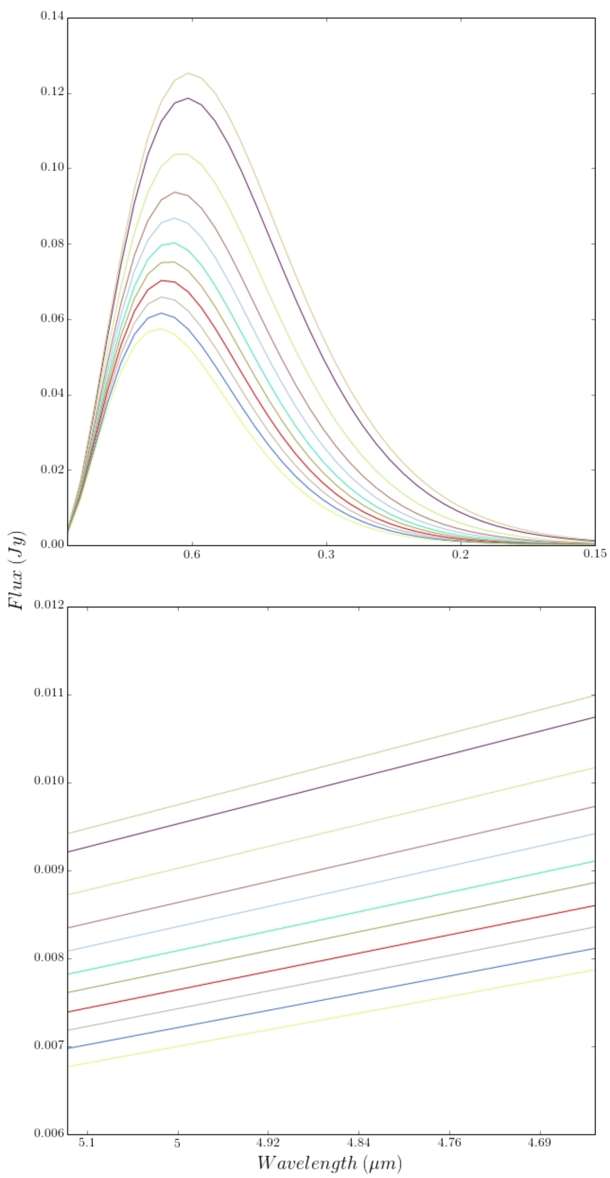

Figure 10. TOP: Theoretical blackbody curve for a temperature range of $6440K$ to $8200K$, scaled for distance.
BOTTOM: Theoretical blackbody curve on the wavelength range for which we have CO data. All calculated curves shown use a radius of $2.6R_\odot$, an upper limit to theoretical radius.

Analysis performed on the region of the the spectrum showing evidence of H_2O absorption was more qualitative, and aimed to determine whether the H_2O absorption lines were shifted as severely as the CO features; i.e., whether the H_2O features were from absorption along the outflow, or arose from the circumstellar disk.

Analysis was primarily performed by comparison between data from LkHα 225S and AS 205A, which is known to have H_2O features in the same wavelength range (for detailed discussion, see Salyk et. al., 2008). Inverting the AS 205A emission spectrum, and correcting for source velocity (v_{lsr} = 4.4 km/s v_{helio} = 7.7 km/s) allows us to form a rough comparison between these data and the source-velocity corrected data for LkHα 225S. We focused primarily on the region of the spectrum from 2.875 μm to 2.945 μm, as it was the most well-studied. Due to the complexity of the spectrum, the previous method of using a Gaussian function to perform a least-squares fit to the observed absorption features fails when applied to these data. Direct empirical comparison between the known AS 205A spectrum and the LkHα 225S spectrum provides a rough first estimate of relative Doppler shifting, suitable for a first approximation of the dynamics of the system. Figure 3 shows the overlay of the AS 205A spectrum (inverted and un-inverted) and the LkHα 225S spectrum.

4. RESULTS AND DISCUSSION

4.1. ^{12}*CO Results*

Analysis of the linecenters for ^{12}CO relative to their theoretical position yields an average blueshift corresponding to -83 ± 8.3 km/s, with a maximum of -70.3 km/s and a minimum of -97.9 km/s. Table 2 shows the name, theoretical center, and calculated velocity of each plotted line.

It is immediately evident that the blueshifting is significant, as can be seen in Figures 1, 4, and 5. Coupled with the data from Matthews (Matthews et al. 2007), which includes a position-velocity diagram indicating no change in velocity with position, we conclude that the region responsible for the ^{12}CO absorption is not a part of the circumstellar disk. Rather, given the velocities and strong absorption features, we conclude that the observed region is seen primarily at this wavelegnth as a molecular outflow from the protoplanetary disk. Coupled with the position-velocity diagram found in (Matthews et al. 2007), we can further conclude that this particular outflow is oriented pole-on.

Other properties of the ^{12}CO emission are difficult to determine using the methods outlined above. Figures 8 and 11 show our attempt at creating a rotation diagram for ^{12}CO absorption. The top plot of Figure 8 is a classical example of a rotation diagram that would be produced by lines with an optical depth $\tau > 1$. Figures 4

Table 2. ^{12}CO Absorption Features; Names, Positions and Velocities

Name	Theoretical Center (μm)	Velocity (km/s)
P(37)	5.053	-97.41
P(36)	5.040	-97.91
P(33)	5.003	-84.61
P(32)	4.991	-95.000
P(31)	4.979	-95.35
P(30)	4.967	-91.75
P(12)	4.774	-80.41
P(11)	4.764	-86.76
P(10)	4.755	-79.96
P(9)	4.745	-70.35
P(8)	4.736	-77.36
P(7)	4.727	-81.16
P(6)	4.718	-81.33
P(5)	4.709	-83.64
P(4)	4.699	-80.37
P(3)	4.691	-77.87
P(2)	4.683	-77.69
P(1)	4.674	-71.25
R(0)	4.657	-73.61
Avg. v (km/s):	-83.36	
σ_v (km/s):	8.333	

and 5 show further evidence that the absorption lines are optically thick at this wavelength range. Both figures here show a double trough in both the individual line and the interpolated lines (Horne & Marsh 1986). This region of the spectrum corresponds to the data points with higher energy in the rotation diagrams of Figure 8. As the full rotation diagram was optically thick, we attempted a linear fit to the apparently linear portion seen in Figure 11. This was unsuccessful, as the optically thick portion extends through the higher energy lines as well. We discovered this only by comparison with the ^{13}CO rotation diagram, which was linear. ^{13}CO showed a column density an order of magnitude greater than the one found by ^{12}CO. This is likely untrue, as relative abundances are such that the optically thick ^{12}CO should have a significantly higher column density. The temperature, likewise, seems to be unreliable. A better model for ^{12}CO is needed, and will be the subject of future work on this region. For reference, Table 3 shows absorption feature names, equivalent widths, and FWHMs.

4.2. ^{13}*CO Results*

Analysis of the linecenters for ^{13}CO was complicated by noise in the spectrum, as well as the close proximity of the absorption features to the much more pronounced ^{12}CO features. We were only able to reliably fit eight absorption features with an adequate Gaussian profile, all in the portion of the spectrum between $\lambda = 4.64$ μm and $\lambda = 4.74$ μm. This analysis yields an average blueshift corresponding to a velocity of -39 ± 3.3 km/s, with a maximum velocity of -31.9 km/s and a minimum velocity of -42.5 km/s. Table 4 shows the name, theoretical center, and calculated velocity shift of the line.

Interestingly, the blueshifting is not comparable to the blueshifts obtained for ^{12}CO, implying that the ^{12}CO

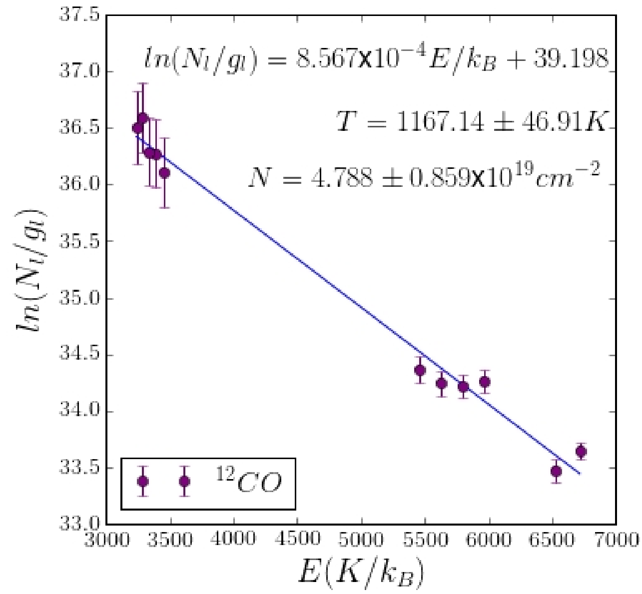

Figure 11. The apparently linear portion of the rotation diagram for ^{12}CO.

Table 3. ^{12}CO Absorption Features; Equivalent Widths, FWHMs, and Associated Errors

Name	Eq. Width (km/s)	$\sigma_{Eq.Wid.}$	FWHM (km/s)	σ_{FWHM}
P(37)	21.37	1.209	105.3	4.047
P(36)	17.44	1.415	61.85	3.188
P(33)	35.11	1.288	112.1	5.646
P(32)	32.71	1.268	105.0	5.274
P(31)	32.44	1.331	100.4	5.531
P(30)	35.49	1.312	94.79	5.825
P(12)	80.60	1.394	91.83	14.54
P(11)	87.79	1.375	98.87	15.23
P(10)	80.90	1.463	87.42	13.61
P(9)	98.61	1.523	106.9	16.48
P(8)	80.15	1.393	84.33	13.79
P(7)	87.69	1.379	78.39	14.18
P(6)	86.88	1.380	85.46	14.77
P(5)	96.69	1.298	93.93	15.74
P(4)	92.47	1.279	89.13	15.08
P(3)	89.99	1.278	86.45	14.74
P(2)	84.29	1.318	78.72	12.82
P(1)	70.99	1.328	81.48	12.05
R(0)	72.18	1.288	82.37	12.04

Table 4. ^{13}CO Absorption Features; Names, Positions and Velocities

Name	Theoretical Center (μm)	Velocity (km/s)
R(3)	4.738	-31.91
R(6)	4.715	-42.47
R(9)	4.693	-40.03
R(10)	4.685	-42.48
R(11)	4.678	-38.81
R(12)	4.671	-39.42
R(13)	4.664	-41.38
R(15)	4.650	-42.47
Avg. v (km/s):	-39.9	
σ_v (km/s):	3.31	

and ^{13}CO features belong to different regions of the object. The blueshift is still significant enough that we can assume with a relatively high degree of certainty that the region responsible for ^{13}CO absorption is also a part of a molecular outflow associated with LkHα 225S.

Unlike ^{12}CO, properties of the ^{13}CO region are somewhat less obscure. Figure 6 shows the interpolated and stacked ^{13}CO absorption features. It is immediately evident in this figure that the ^{13}CO features do not show the same characteristic double well apparent in the ^{12}CO absorption features. This is a good indicator, along with the relative small size of the features in the spectrum that the ^{13}CO absorption lines are not optically thick, as the ^{12}CO lines were. From the rotation diagram, we can derive a column density of the ^{13}CO absorbing region of $(3.3 \pm 1.9) \times 10^{20}$ cm^{-2}. Temperature of the region is the inverse slope of the linear fit, given that values on the x-axis are the quantity $E(K/k_b)$. We can find therefore that the temperature of this region is approximately $(383) \pm 1.35 \times 10^{-4}$, making the region fairly hot with respect to the surrounding medium. For reference, Table 5 shows absorption feature names, equivalent widths, FWHMs, and associated errors in those quantities.

Table 5. ^{13}CO Absorption Features; Equivalent Widths, FWHMs, and Associated Errors

Name	Eq. Width (km/s)	$\sigma_{Eq.Wid.}$	FWHM (km/s)	σ_{FWHM}
R(3)	4.316	1.588	18.29	1.823
R(6)	5.658	1.587	23.92	2.019
R(9)	5.172	1.455	21.11	1.796
R(10)	5.185	1.448	27.93	1.752
R(11)	4.278	1.439	21.52	1.509
R(12)	4.779	1.441	23.64	1.643
R(13)	4.194	1.393	24.37	1.411
R(15)	2.909	1.370	26.75	1.164

4.3. *H_2O Results*

We inverted and exaggerated the emission line spectrum for AS 205A to obtain a spectrum that closely resembled the spectrum obtained for LkHα 225S. It was immediately evident that there was again significant blueshifting of the H_2O absorption features, as there were in ^{12}CO and ^{13}CO. The spectrum obtained here had a much higher noise level than the spectra obtained for CO. We used the region of the spectrum for AS 205A between $\lambda = 2.925$ μm and $\lambda = 2.932$ μm, which showed several prominant H_2O features (Salyk et al. 2008) to align the LkHα 225S spectrum. In the end, a shift of $\approx$ 0.3 nm was needed to align the LkHα 225S spectrum with the AS 205A spectrum. At this wavelength, this corresponds to a Doppler shift of -30.91 km/s, less than both ^{12}CO and ^{13}CO, but still larger than what would be expected from the protoplanetary disk, implying that it, along with the other absorption features, is propelled by a molecular outflow originating from LkHα 225S. This is a significant find, as it is thought that it may be difficult for H_2O to survive in the radiative environment of an outflow. Further study of this spectrum is needed to confirm our findings, and derive a model that accurately explains the observed phemonenon.

4.4. *Geometry of the LkHα 225S Molecular Outflow*

Having obtained a set of Doppler lineshifts and linewidths, our next goal was to determine some properties of the geometry of the region, in order to further our understanding of the nature of the outflow. Models tend to agree that the outflow spirals with a constant angular momentum. This is evident in our linewidths, which correspond to the azimuthal motions in the outflow. Therefore, we expect $v_\phi r = const.$, and that $v_\phi \propto \frac{1}{r}$. Having obtained a set of linewidths for ^{12}CO and ^{13}CO, we can compare the ratio of azimuthal velocities (linewidths) to determine the ratio of distances along the outflow stream. Table 6 shows comparisons between median, mean, minimum, and maximum azimuthal velocities.

Table 6. Comparison of ^{12}CO and ^{13}CO azimuthal velocities by linewidth comparisons

	Linewidth (^{12}CO)	$R_{^{13}CO}/R_{^{12}CO}$
Median v	89.131	0.267
Mean v	90.771	0.258
Max. v	112.123	0.249
Min. v	61.854	0.296
	Linewidth (^{13}CO)	
Median v	23.78	
Mean v	23.44	
Max. v	27.93	
Min. v	18.29	

Variations between calculated ratios of radii were minimal, and were all around $R_{^{13}CO}/R_{^{12}CO} \approx 0.27$. In all cases, the ^{13}CO absorption features appear to be more interior to the disk than the ^{12}CO features.

Additionally, tangential velocity is expected to increase with distance from the origin of the outflow due to radiative acceleration. To determine the relative distances of our three studied spectra, we used models from Kurosawa, Harries, and Symington (Kurosawa et al. 2005), who give radius as a function of wind acceleration parameter, β. Interestingly, in this model, for $\beta = 0.2$, H_2O would be interior to the disk. However, for all other values of the parameter β, H_2O is the most interior to the disk, while still being within the outflow. In this model, ^{12}CO is the most exterior of the three molecules studied, and H_2O is the most interior, while ^{13}CO falls between the two. Table 7 shows the ratios of radii between the three molecules, relative to ^{12}CO.

Table 7. Comparison of ^{12}CO, ^{13}CO, and H_2O tangential velocities by comparison of Doppler shifts

^{12}CO	$v_{avg} = 83$ km/s		
Accel. Param. β	l_{AU}		
0.2	0.0103		
0.5	0.019		
1	0.12		
2	0.1665		
^{13}CO	$v_{avg} \approx 40$ km/s		
β	l_{AU}	$R_{^{13}CO}/R_{^{12}CO}$	
0.2	1.1×10^{-4}	0.011	
0.5	1.1×10^{-2}	0.58	
1	0.1	0.83	
2	0.115	0.697	
H_2O	$v_{avg} \approx 31$ km/s		
β	l_{AU}	$R_{H_2O}/R_{^{12}CO}$	$R_{H_2O}/R_{^{13}CO}$
0.2	N/A	N/A	N/A
0.5	0.01	0.53	0.91
1	1.6×10^{-2}	0.13	0.16
2	0.11	0.67	0.96

5. DISCUSSION AND CONCLUSIONS

From the obtained spectra of the LkHα 225S region, we were able to derive several interesting quantities about the region. The region appears to be a molecular outflow, oriented to be pole-on, originating at the protostar at the center of the region. This hypothesis is supported by the significant blueshift in the absorption features for ^{12}CO, ^{13}CO, and H_2O. Furthermore, this hypothesis is supported by the research of other groups, such as Matthews et. al. (Matthews et al. 2007), who give a position-velocity diagram indicative of a single, blueshifted source with no variation in velocity with position, whereas for features endemic to the protoplanetary disk, we would expect to see both a red- and blueshifted component on a position-velocity diagram.

This is especially interesting in the case of H_2O absorption, as the H_2O absorption features are likewise blueshifted in such a way as to imply that they too originate in the same molecular outflow, despite the current model that suggests H_2O would be unable to survive the energetic outflow regions.

While all three molecules showed significant Doppler shifting in their absorption features relative to the theoretical positions of those same features, all three showed different levels of shifting. From this, we conclude that all three sets of absorption features likely originate in different areas of the outflow. Using models for radiative acceleration along a molecular outflow, we found that H_2O was most interior to the protoplanetary disk, while ^{12}CO was most exterior, and ^{13}CO fell between the two. We were also able to derive a ratio of radii for ^{12}CO and ^{13}CO using the conservation of angular momentum. Using this calculation, we showed that ^{13}CO was interior to ^{12}CO, but values were not comparable to the values given by the radiative acceleration model. We theorize this is due to the optical depth of the ^{12}CO absorption features, which likely caused inaccuracies in directly observing linewidths.

Due to the same saturation, we were unable to use a rotation diagram to derive the temperature and column density of the ^{12}CO absorbing region. Further work includes finding a new model that will allow us to derive these quantities despite the absorption features being optically thick. The rotation diagram for ^{13}CO, however, appears to be optically thin, and we were able to derive column density and temperature for the absorbing ^{13}CO. The temperature for ^{13}CO derived from the rotation diagram was $T = (383.1) \pm 1.3 \times 10^{-4} K$, with a ^{13}CO column density of $N = (3.25 \pm 1.88) \times 10^{20} cm^{-2}$.

Finally, we determined that the continuum emission for this source could not originate at the star. Despite the lack of relevant data for this region, for our purposes we found that even the most extreme assumptions we made concerning the system yielded a continuum level two orders of magnitude below the observed value. Using the derived temperature of the ^{13}CO region, we were able to place a lower bound on the radius of the continuum region of $\approx 13AU$. The derived temperature here would be an extreme upper bound to the temperature of the continuum emission, as the ^{13}CO is expected to be significantly different in temperature than the continuum region due to its placement within the outflow. We can safely say that given our assumptions, the continuum must come from a much larger area than could be provided by the protostellar object at the center of the region, and that the protoplanetary disk must therefore be providing the majority of the continuum emission.

In summary, our observations seem to be of a pole-on molecular outflow within the LkHα 225S region. We observe several different molecules at a variety of wavelength ranges and find their absorption features to all be significantly Doppler shifted relative to their theoretical positions. The calculated Doppler shifts show three separate and distinct regions along the column of this outflow, each with its own separate properties. The widths of the ^{12}CO and ^{13}CO absorption features differ in a manner consistent with the expected conservation of angular momentum at various distances along the column of the outflow, further supporting the hypothesis that these two molecules are in distinct regions separate from one another.

Further research is needed to confirm our findings, and test our Doppler-derived velocities. Other future work includes building a model that can adequately explain the survival of the H_2O molecule in the energetic outflow region, and building a model that allows us to derive useful quantities from the ^{12}CO absorption features, despite their opacity to continuum light. Eventually, our goal to compare densities along the column of the outflow to further our understanding of the physics driving these molecular outflows, and perhaps refine our understanding of the nature of these features of protoplanetary disks, including the driving impulse behind the outflow itself.

6. ACKNOWLEDGEMENTS

The author would like to thank Dr. Colette Salyk for her efforts to bring this paper into being, as well as her advice, and not the least, obtaining the data used in this paper. We thank also the Vassar College Physics and Astronomy Department for the opportunities afforded to us to perform research in a supportive environment.

REFERENCES

Aspin, C., Sandell, G., & Weintraub, D. 1994, Astronomy and Astrophysics, 282, L25

Bally, J., Morse, J., & Reipurth, B. 1996, Science with the Hubble Space Telescope, STScI, p.491

Fairlamb, J., et al. 2015, Mon. Not. R. Astron. Soc., 453, 976

Herbig, G. H. 1960, Astrophysical Journal Supplement, 4, p.337

Herbst, W., & Shevchenko, V. 1999, The Astronomical Journal, 118, 1043

Hillenbrand, L. A., et al. 1995, The Astronomical Journal, 109, 280

Horne, K., & Marsh, T. 1986, Mon. Not. R. Astron. Soc., 218, 761

Kenyon, S. J., & Hartmann, L. 1995, Astrophysical Journal Supplement, 101, 117

Kurosawa, R., Harries, T. J., & Symington, N. H. 2005, Mon. Not. R. Astron. Soc., 370, 580

Lenz, D. D., & Ayres, T. R. 1992, Publications of the Astronomical Society of the Pacific, 104, p.1104

Matthews, B. C., et al. 2007, The Astrophysical Journal, 671, 483

Mora, A., et al. 2001, Astronomy and Astrophysics, 378, 116

Mundy, L. G. 1999, ASTRO 688: Molecules, Dust, Molecular Clouds, and Star Formation (unpublished)

Palla, F., et al. 1995, Astronomy and Astrophysics, 293, 521

Salyk, C., Blake, G., Boogert, A., & Brown, J. 2011, The Astrophysical Journal, 743, 112

Salyk, C., et al. 2008, The Astrophysical Journal Letters, 676, L49

Shevchenko, V., Ibragimov, M., & Chernysheva, T. 1991, Soviet Astronomy, 35, 229

Zhang, K., et al. 2015, The Astrophysical Journal, 805

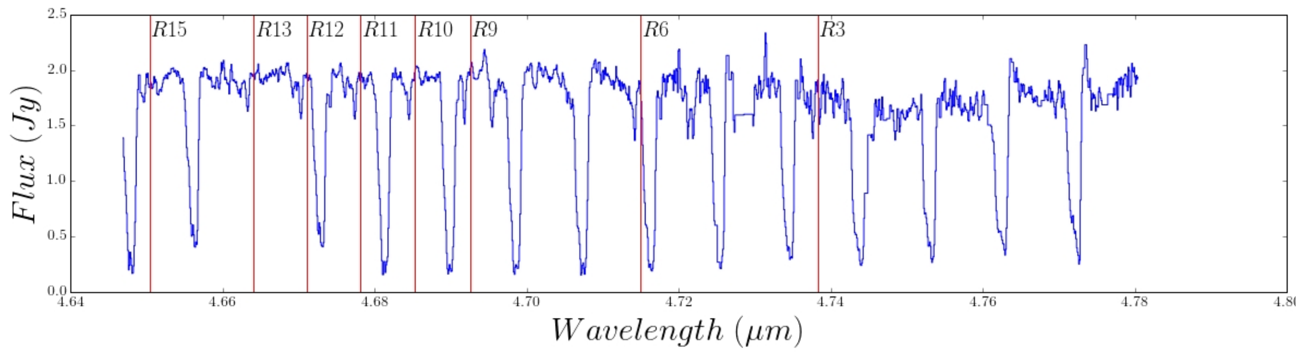

Figure 12. The spectrum for LkHα 225, overlaid with ^{13}CO line positions in red. In this version, we have not corrected for the outflow velocity in this region, in order to provide a point of contrast with the outflow-corrected version seen in Figure 2.